JOURNAL OF GEOPHYSICAL RESEARCH, VOL. 106, NO. A3, PAGES 3783–3798, MARCH 1, 2001

Geospace Environment Modeling magnetic reconnection challenge: Simulations with a full particle electromagnetic code

P. L. Pritchett

Department of Physics and Astronomy, University of California, Los Angeles

Abstract. The objective of the Geospace Environment Modeling (GEM) magnetic reconnection challenge is to understand the collisionless physics that controls the rate of magnetic reconnection in a two-dimensional configuration. The challenge involves investigating a standard model problem based on a simple Harris sheet configuration by means of a variety of physical models in order to isolate the essential physics. In the present work the challenge problem is modeled using an electromagnetic particle-in-cell code in which full particle dynamics are retained for both electrons and ions and Maxwell's equations are solved without approximation. The timescale for reconnection is of the order of 10 Ω_i^{-1} (where Ω_i is the ion cyclotron frequency based on the asymptotic field B_0), and the corresponding reconnection electric field is $(c/v_A)E_y/B_0 \sim 0.24$. The diffusion region near the neutral line is observed to develop a multiscale structure based on the electron and ion inertial lengths c/ω_{pe} and c/ω_{pi}. The difference between the ion and electron dynamics in the diffusion region gives rise to in-plane (Hall) currents which produce an out-of-plane B_y field with a quadrupolar structure. In the diffusion region the magnetic field is no longer frozen-in to the electrons; the inductive E_y field is supported primarily by the off-diagonal electron pressure terms in the generalized Ohm's law. The reconnection rate is found to be insensitive to electron inertia effects and to the presence of a moderate out-of-plane initial field component $B_{0y} \lesssim B_0$. The results are consistent with the theory that the reconnection rate is independent of the mechanism which breaks the frozen-in condition and is controlled by dynamics at length scales much greater than the electron dissipation region.

1. Introduction

Magnetic reconnection enables a magnetized plasma to convert magnetic energy into high-speed flows and thermal energy, and it is one of the most important transport mechanisms in plasmas. In the magnetosphere, reconnection at the dayside magnetopause facilitates the input of mass, energy, and momentum into the magnetosphere, and reconnection processes in the geomagnetic tail are involved in storm and substorm dynamics. Magnetic reconnection relies on the presence of a dissipation mechanism in a localized region of space, the so-called diffusion region. In a sufficiently collisional plasma, resistive MHD theory is valid for describing this region and determining the reconnection rate [*Parker*, 1957; *Sweet*, 1958; *Furth et al.*, 1963]. In collisionless reconnection, such as is involved in magnetospheric reconnection, it is electron inertia that allows the frozen-in flux constraint to be broken [*Laval et al.*, 1966; *Vasyliunas*, 1975], and the structure of the diffusion region is modified by kinetic Alfvén and whistler dynamics [e.g., *Drake*, 1995].

The objective of the Geospace Environment Modeling (GEM) magnetic reconnection challenge is to identify the collisionless physics that controls the rate of magnetic reconnection. The general approach and motivation are set forth in the overview paper by *Birn et al.* [this issue]. The procedure adopted in the challenge is to investigate a standard model problem based on a simple *Harris* [1962] sheet configuration by means of a variety of numerical models: resistive MHD, Hall MHD, hybrid (electrons treated as a fluid, ions treated as particles), and full particle models. The present work presents results for the GEM challenge obtained using an electromagnetic particle-in-cell code in which full particle dynamics are retained for both the electrons and ions and Maxwell's equations are solved without approximation. The comparison between the results obtained with the various models is given in the overview paper [*Birn et al.*, this issue].

There is one feature of the GEM configuration that should be noted at the outset. The Harris current

Paper number 1999JA001006.
0148-0227/01/1999JA001006$09.00

sheet is modified by including a moderately large magnetic field perturbation, which produces an initial island whose width is comparable to the initial width of the current layer. The reason for this is to put the system in the nonlinear regime of magnetic reconnection at the outset and thus avoid the well-known dependence of the linear growth of the tearing mode on the precise form of the dissipation. In the nonlinear regime this dependence on the dissipation mechanism is expected to be, and indeed proves to be [*Birn et al.*, this issue], greatly reduced. As a consequence of this initial perturbation, the present studies do not address any of the issues concerning reconnection onset, including the contentious issue of whether the collisionless tearing mode is unstable or not in the presence of a finite normal magnetic field [*Lembège and Pellat*, 1982; *Pellat et al.*, 1991; *Brittnacher et al.*, 1994; *Quest et al.*, 1996; *Sitnov et al.*, 1998].

The outline of the paper is as follows. Section 2 describes the particle-in-cell simulation model, while section 3 presents the results for the GEM challenge problem. Section 4 examines the effects on the reconnection rate of including an out-of-plane component in the intial magnetic field configuration (the so-called guide field) and varying the level of the uniform background density. Section 5 gives a summary of the present results and places them in the context of the overall GEM challenge.

2. Simulation Model

The present study employs a 2 1/2-dimensional (two spatial dimensions, all three velocity components) electromagnetic particle simulation model which retains the full dynamics for the electrons as well as the ions [*Pritchett et al.*, 1996]. In this model the electric and magnetic fields are obtained by integrating the time-dependent Maxwell equations:

$$\partial \mathbf{E}/\partial t = c\nabla \times \mathbf{B} - 4\pi \mathbf{J}, \tag{1}$$

$$\partial \mathbf{B}/\partial t = -c\nabla \times \mathbf{E} \tag{2}$$

forward in time using an explicit leapfrog scheme in which $\mathbf{E}$ is defined at half-integral time steps and $\mathbf{B}$ is defined at integral time steps. The relativistic particle equations of motion are likewise integrated in time using a leapfrog scheme, with the particle coordinates defined at the half-integral times and the momenta at integral times. The current density $\mathbf{J}$ appearing in (1) is accumulated on a spatial grid from the particle data. Such a model makes no approximations to the basic physical laws, and it thus constitutes the most complete and fundamental model for the numerical representation of a collisionless plasma.

The solution of (1) and (2) will automatically satisfy Poisson's equation $\nabla \cdot \mathbf{E} = 4\pi\rho$ provided that the charge conservation condition $\partial\rho/\partial t = -\nabla \cdot \mathbf{J}$ is maintained by the numerical algorithm. There are two alternative approaches to satisfying this condition. One is to employ a rigorous charge conservation scheme for the current deposition [*Villasenor and Buneman*, 1992; *Wang et al.*, 1995], while the other [e.g., *Langdon and Lasinski*, 1976] involves adding a correction $\delta\mathbf{E}$ to the electric field computed from (1) determined by solving

$$\nabla^2(\delta\phi) = -(4\pi\rho - \nabla \cdot \mathbf{E}) \tag{3}$$

and setting $\delta\mathbf{E} = -\nabla\delta\phi$. We employ this second method.

The spatial storage of $\mathbf{E}$ and $\mathbf{B}$ is based on the *Yee* [1966] lattice, which is a fully staggered grid mesh system. The components of $\mathbf{E}$ and $\mathbf{J}$ are defined at midpoints of cell edges, while the components of $\mathbf{B}$ are defined at the midpoints of the cell surfaces [see *Wang et al.*, 1995, Figure 1]. This scheme has the advantage of removing the spatial averaging that is required in the solution of (1) and (2) when a single staggered system is used where all the components of $\mathbf{E}$ are defined at the center point of the $\mathbf{B}$ mesh.

As described by *Birn et al.* [this issue], the initial configuration for the present study is a Harris neutral sheet in the x,z plane. The initial magnetic field is $\mathbf{B}_0 = B_{0x}(z)\hat{\mathbf{x}}$, with

$$B_{0x}(z) = B_0 \tanh(z/w), \tag{4}$$

and the corresponding density is

$$n_0(z) = n_0 \mathrm{sech}^2(z/w) + n_b, \tag{5}$$

where w is the half thickness of the current sheet and n_b represents a background density component which provides a floor to the density. The equilibrium conditions for the neutral sheet require that

$$B_0^2/8\pi = n_0(T_{e0} + T_{i0}), \tag{6}$$

$$w = (2c/eB_0)(T_{e0} + T_{i0})/|V_{i0} - V_{e0}|, \tag{7}$$

where T_{e0} and T_{i0} are the (uniform) electron and ion temperatures of the Maxwellian particle distributions, and the particle drifts in the y direction satisfy $V_{e0}/V_{i0} = -T_{e0}/T_{i0}$. The background plasma component has no drift, and the background temperatures for the electrons and ions are assumed to be the same as T_{e0} and T_{i0}, respectively.

The dimensions of the present problem are $L_x \times L_z = 25.6c/\omega_{pi} \times 12.8c/\omega_{pi}$, where the ion inertial length c/ω_{pi} is defined using the peak Harris density n_0. The half thickness $w = 0.5c/\omega_{pi}$, the background density $n_b = 0.2n_0$, the temperature ratio is $T_e/T_i = 0.2$, and the mass ratio is $m_i/m_e = 25$. The ion drift V_{i0} for the Harris particles is then $1.67v_A$, where v_A is the Alfvén speed based on B_0 and n_0. The results to be discussed here employ a $N_x \times N_z = 512 \times 256$ simulation grid, so that the spatial resolution is $\Delta x = \Delta z = 0.05c/\omega_{pi} = 0.25c/\omega_{pe}$. Preliminary runs with a grid spacing twice as large ($0.10c/\omega_{pi} = 0.50c/\omega_{pe}$) were not quite ade-

quate to resolve all of the structure in the problem. The speed of light is chosen so that $c/v_A = 20$, and the electron Debye length is $\lambda_{De} = 0.3\Delta x$. The time step is taken to be $\omega_{pe}\Delta t = 0.15$, or equivalently $\Omega_i\Delta t = 0.0015$. The durations of the simulations are typically $\Omega_i t = 30$, corresponding to 20,000 time steps. The primary run to be discussed here employed 2.00 million particles per species to represent the Harris distribution. This corresponds to a peak density $n_0 = 195$ particles per cell. In order to reduce the running time and memory requirements the background plasma (an additional 2.56 million particles per species) had charge and mass twice as large as for the respective Harris particles. Some additional runs will be discussed that employed one half as many particles over the same grid size.

3. Results for the GEM Challenge Problem

As explained by *Birn et al.* [this issue], the Harris neutral sheet configuration is modified by including an initial flux perturbation of the form

$$\psi(x,z) = -\psi_0 \cos(2\pi x/L_x)\cos(\pi z/L_z), \qquad (8)$$

where ψ is the vector potential component A_y. This produces a substantial magnetic island (transverse size comparable to the initial half width w) with the X line at $x = 0$, $z = 0$ (the center of the simulation region) and ensures that the evolution of the system will be dominated by a mode whose scale is that of the entire

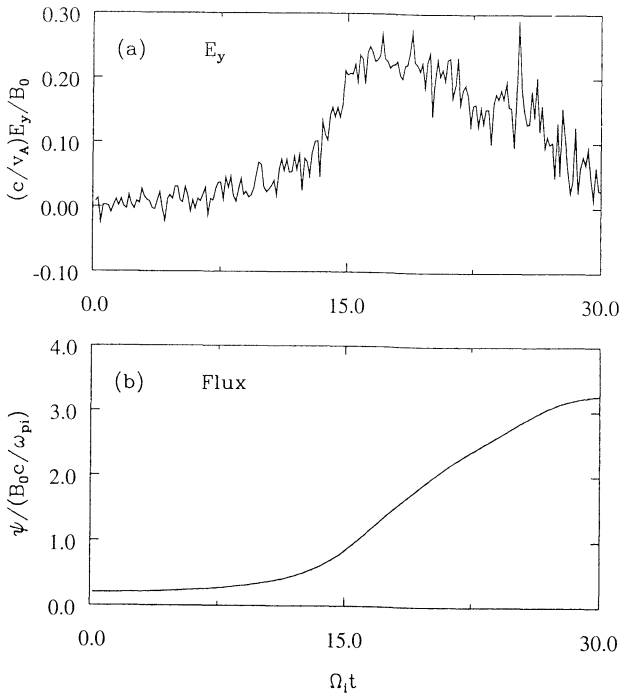

Figure 1. Time history of (a) the induction electric field E_y at the X line and of (b) the reconnected magnetic flux $\Delta\psi$ in the Geospace Environment Modeling (GEM) reconnection challenge problem.

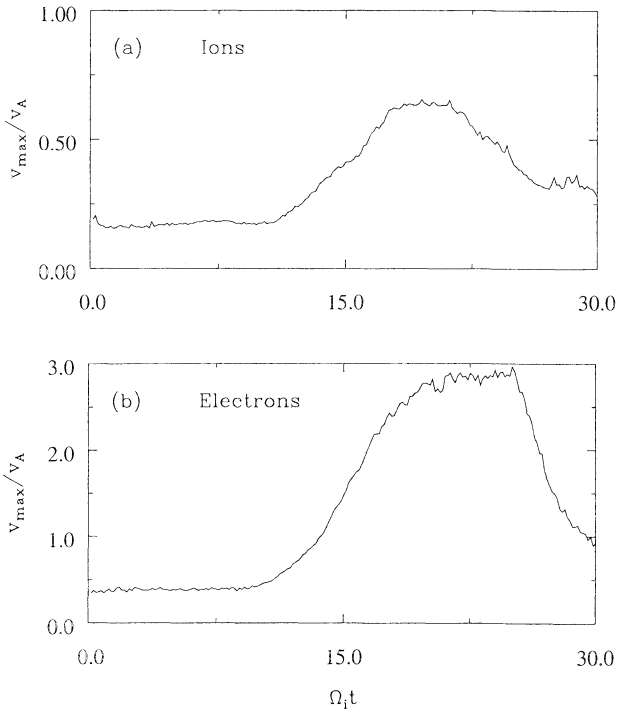

Figure 2. Time history of the maximum in-plane (x,z) (a) ion and (b) electron bulk flow speeds.

axis length L_x rather than by the fastest growing tearing mode of the Harris configuration whose wavelength is $\approx 6c/\omega_{pi}$. In addition, the use of the initial perturbation emphasizes the nonlinear stage of the reconnection process. The value chosen for ψ_0 is $\psi_0/(B_0c/\omega_{pi}) = 0.1$. The uniform drifts V_{i0} and V_{e0} for the Harris particles in the simulation are modified to reproduce the current perturbation contained in (8) so that $\nabla \times \mathbf{B} = 4\pi\mathbf{J}/c$ remains satisfied using the current density computed from the particle distributions. The corresponding relative force imbalance ($\mathbf{J} \times \mathbf{B}/c \neq \nabla P$) is only a few percent at the center of the sheet and becomes significant only in the outer region of the Harris profile where the number density has dropped to a few particles per cell. This imbalance is readily compensated for in the initial steps of the simulation.

Figure 1 shows the time evolution of the induction electric field E_y at the X line and of the reconnected magnetic flux $\Delta\psi$. This latter quantity is the flux difference between the O and X lines; the initial value of $\Delta\psi \equiv 2\psi_0 = 0.2B_0c/\omega_{pi}$. The E_y field, which is somewhat noisy, increases slowly at first; the flux difference $\Delta\psi$ does not reach the value 0.5 until $\Omega_i t = 12.4$. E_y then increases more rapidly and reaches a maximum value of $(c/v_A)E_y/B_0 \approx 0.24$ for $\Omega_i t \approx 18$; $\Delta\psi/(B_0c/\omega_{pi}) = 1.0$ at $\Omega_i t = 15.7$ and $= 1.5$ at $\Omega_i t = 17.9$. E_y then decreases back toward zero, and $\Delta\psi$ reaches a final value of $\approx 3.2B_0c/\omega_{pi}$. Figure 2 shows time history plots of the maximum in-plane ion and electron bulk flow speeds. Normalized to the Alfvén speed, the ion speed reaches a peak value of $\approx$0.65, while

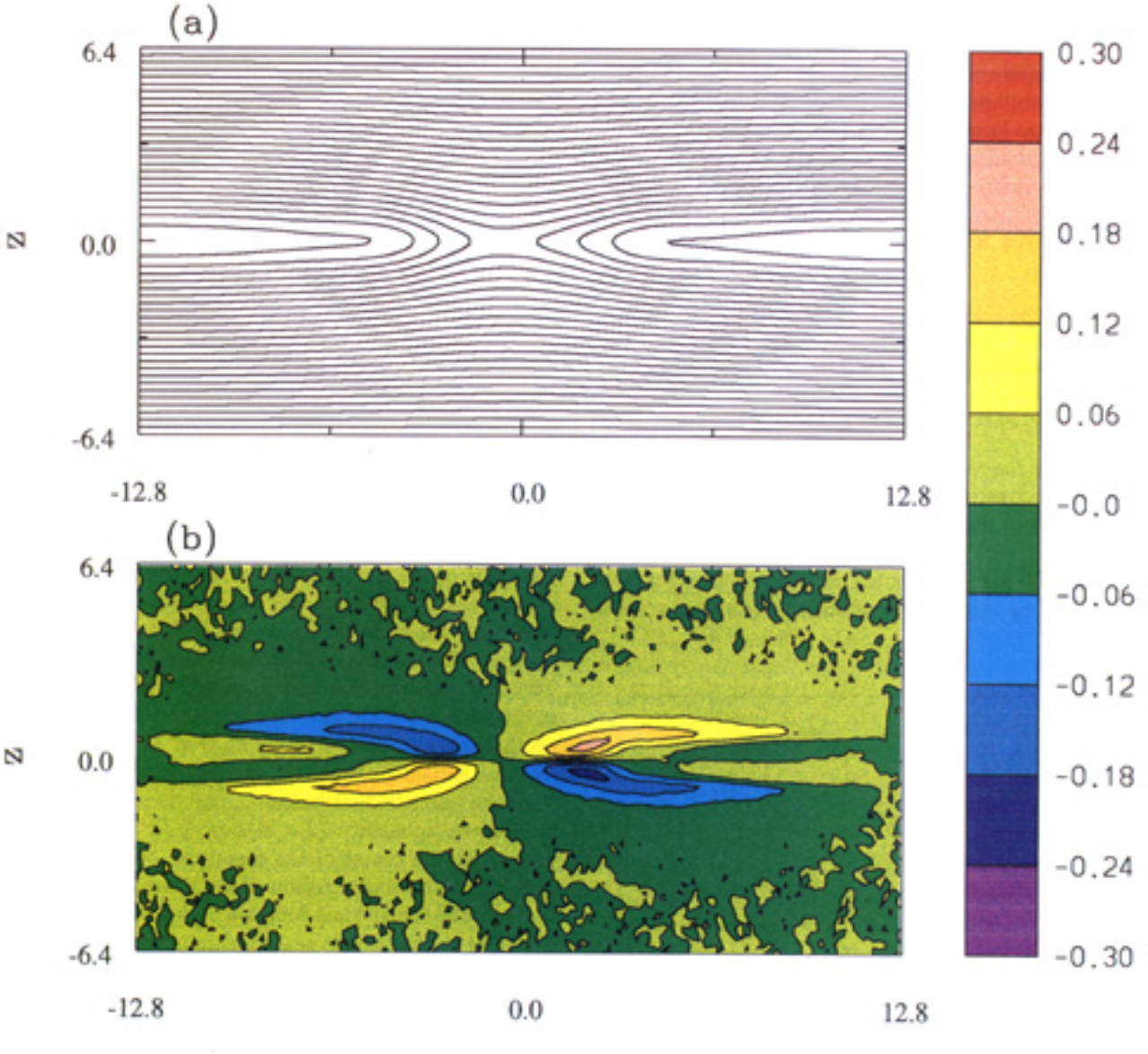

Plate 1. (a) Magnetic field lines in the x,z plane and (b) contours of the out-of-plane B_y field at the time when $\Delta\psi = 1.0 B_0 c/\omega_{pi}$ ($\Omega_i t = 15.7$).

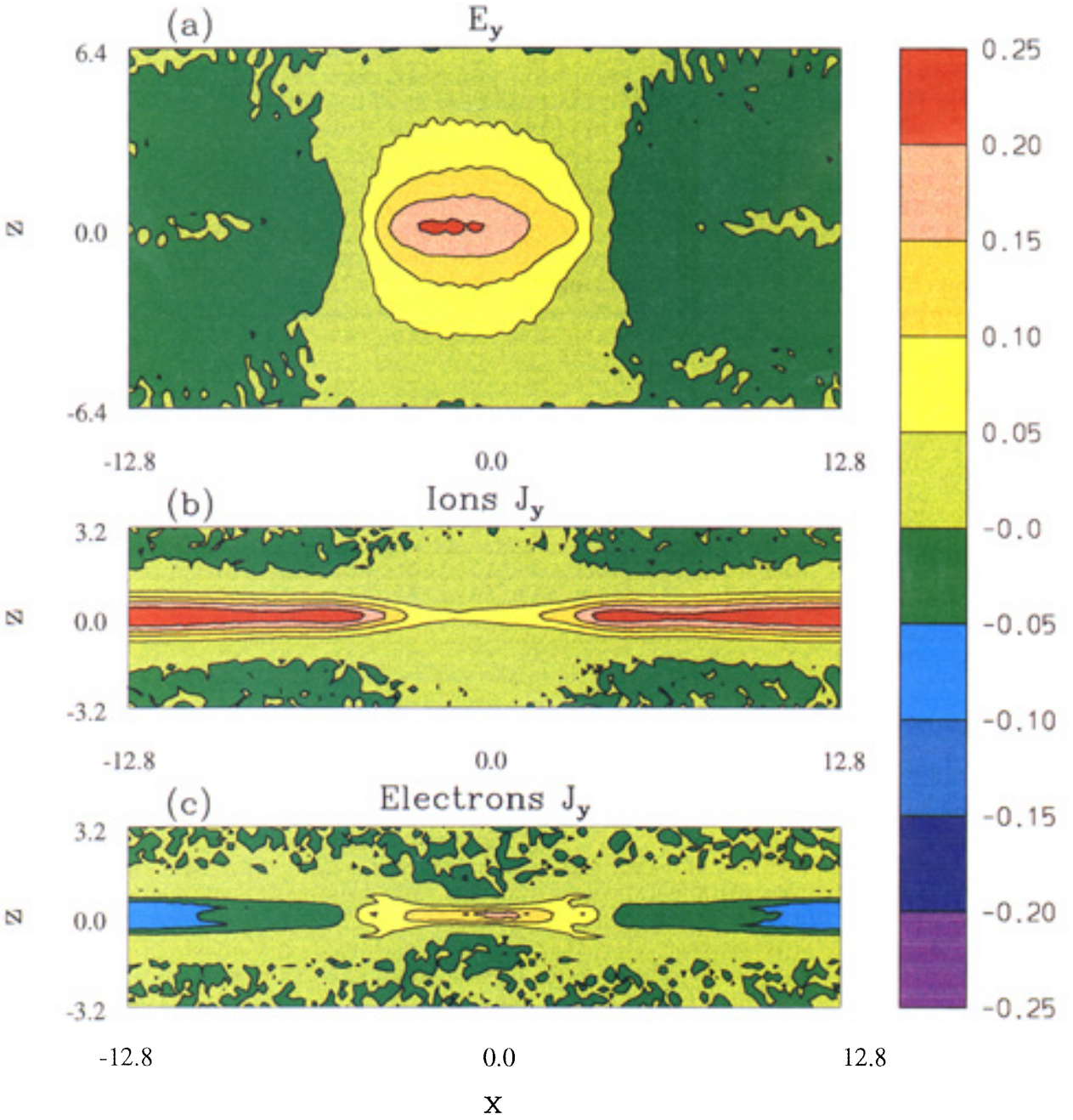

Plate 2. (a) The inductive electron field E_y averaged over the interval from $\Omega_i t = 15.0$ to 15.6 and the (b) ion and (c) electron current density J_y at $\Omega_i t = 15.7$.

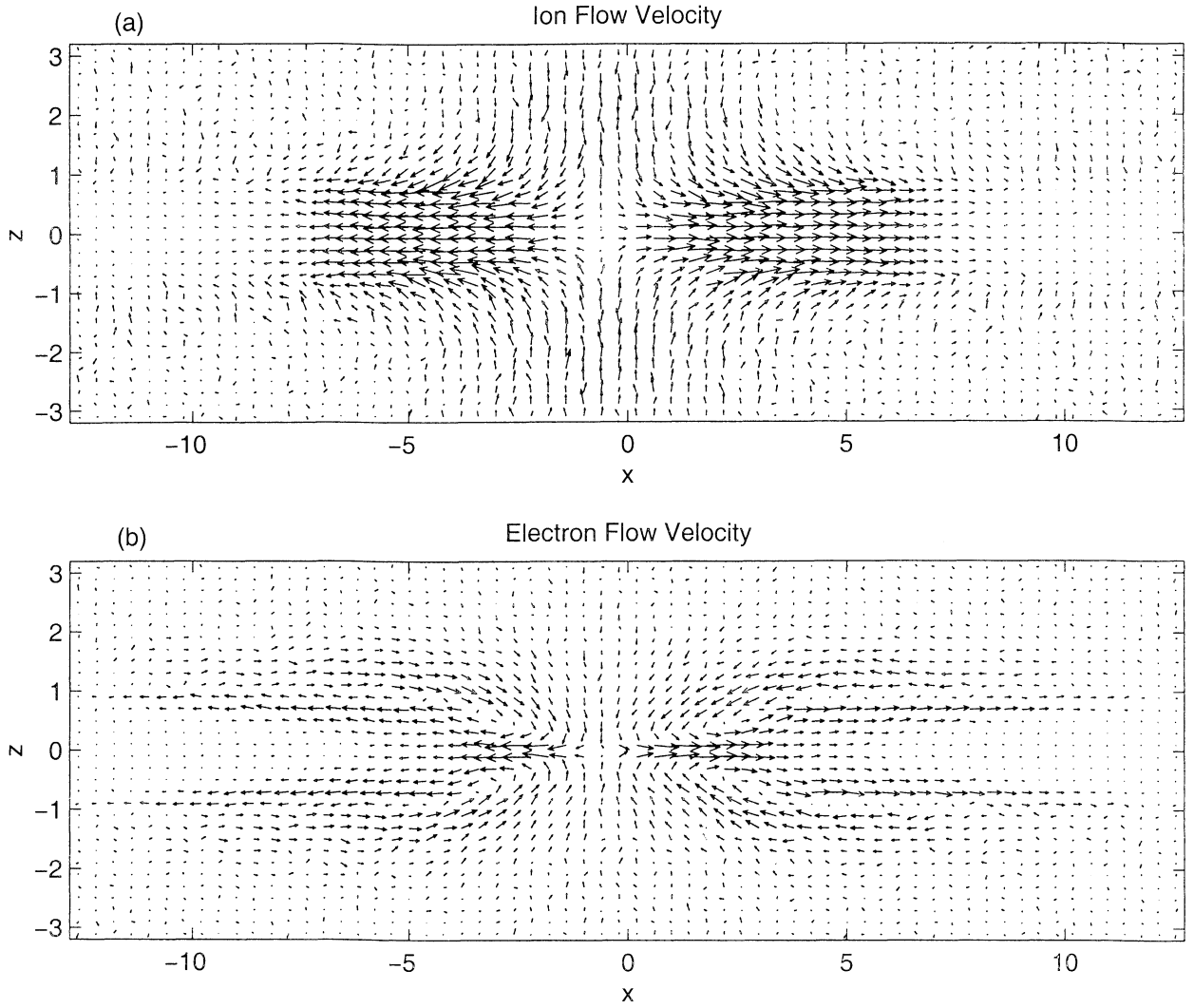

Figure 3. The in-plane (x,z) (a) ion and (b) electron flow velocities at the same time as in Plate 1.

the electron top speed is ≈2.8. Both speeds decrease as the reconnection rate drops back to zero.

Plate 1 shows magnetic field lines in the x,z plane and contours of the out-of-plane B_y field at the time when $\Delta\psi = 1.0B_0c/\omega_{pi}$ ($\Omega_i t = 15.7$). This is shortly before the time of the peak reconnection rate. The maximum island width is now $\approx c/\omega_{pi}$. The B_y field exhibits the characteristic quadrupole pattern that is expected due to the in-plane Hall currents [*Sonnerup*, 1979; *Terasawa*, 1983]. (Note that the positive y direction is into the page.) The region of significant B_y is confined within the magnetic island structure, and the peak value of $|B_y|$ is $\approx 0.2B_0$. The maximum value of $|B_y|$ occurs at $|x| \approx 2.5c/\omega_{pi}$ away from the neutral line. At later times the B_y wings expand in z as the island grows; the maximum value remains about the same. Some additional B_y fields are also formed at the later times near the $z = 0$ line and closer to the x boundaries; these structures may be spurious owing to the assumption of periodic boundary conditions.

Figure 3 shows the in-plane ion and electron flow velocities at the same time as for Plate 1. The inflow toward the neutral line is driven by the inductive electric field (into the plane of the figure) in the form of an $\mathbf{E} \times \mathbf{B}$ drift. The ions become demagnetized and begin to flow outwards at a distance $|z| \sim c/\omega_{pi}$ away from the neutral line. The electron inflow, on the other hand, persists to a much shorter distance $\sim c/\omega_{pe}$ before being diverted. The electrons are then expelled at super-Alfvénic speeds out of the diffusion region within this narrow layer. Outside of the diffusion region the electron flow is a maximum along the separatrix; at larger values of $|z|$, there is a return electron flow back toward the diffusion region.

Plate 2a shows the inductive electric field E_y averaged over the time interval from $\Omega_i t = 15.0$ to 15.6. The region of enhanced field is roughly circular centered on the X line and has a radius of $\approx 4c/\omega_{pi}$. Plates 2b and 2c show the ion and electron current density J_y at $\Omega_i t = 15.7$. At time $t = 0$, J_y for the Harris distribution

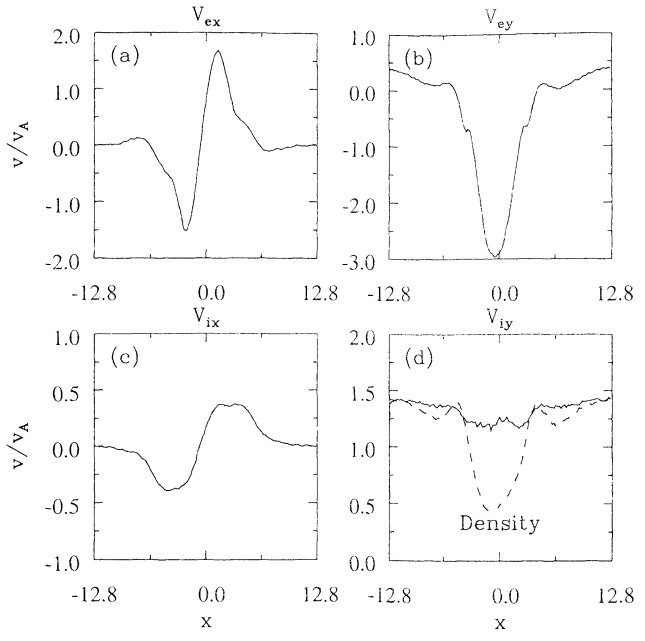

Figure 4. Velocity profiles averaged over the interval from $\Omega_i t = 15.0$ to 15.6 as a function of x at $z = 0$ for (a) electron V_x, (b) electron V_y, (c) ion V_x, and (d) ion V_y. The dashed line in Figure 4d shows the ion number density as a function of x at the same time.

is independent of x, is positive (directed into the page) everywhere, and the ion current density is five times as large as the electron current density. As shown in Plate 2, the role of the electron and ion currents is reversed in the elongated (in x) diffusion region around the X line. Here the electron current dominates over the ion current by a factor of ~2.5. This is a result of the large increase in the electron drift in the y direction (by about a factor of 9 compared to the initial value) produced by the inductive E_y field. As shown in Figure 4, the magnitude of the electron drift in y peaks near the X line and remains enhanced out to $|x| \approx 3$–$4c/\omega_{pi}$; in contrast, the ion drift is nearly constant over this region and is ~10% smaller than its initial value. This effect is qualitatively similar to simulation results that have shown that thin electron current sheets form within ion-dominated current sheets in response to an external driving convection electric field [*Pritchett and Coroniti*, 1995; *Hesse et al.*, 1996]. Outside of the diffusion region the ion current remains dominant throughout the rest of the magnetic island and is only slightly increased from its initial value (due to an increased density). Here the electron current is in the opposite direction to that of the ions. While the island size in z is of the order of the ion inertial length c/ω_{pi}, the intense electron current in the diffusion region is limited to a much narrower region of half thickness 1–$2c/\omega_{pe}$. In this region the electrons are expelled at super-Alfvénic speeds (see Figures 3 and 4) away from the X line out to a distance of $\approx 3c/\omega_{pi}$. The ion flow is much slower but persists out to $\approx 5c/\omega_{pi}$ before equality in the electron and ion speeds is reestablished.

As is shown in Plate 2, the inductive field E_y is a maximum in the region around the X line where the magnetic field is very small. It is thus instructive to examine the physics that supports this field. Assuming a two-fluid model for the plasma, one obtains directly from the electron momentum equation without further approximation that

$$\mathbf{E} = -\frac{1}{c}\mathbf{v}_e \times \mathbf{B} - \frac{\nabla \cdot \underline{\mathbf{P}}_e}{en_e} - \frac{m_e}{e}\frac{d\mathbf{v}_e}{dt}, \tag{9}$$

where $\underline{\mathbf{P}}_e$ is the electron pressure tensor. If we use $\mathbf{J} = e(n_i\mathbf{v}_i - n_e\mathbf{v}_e)$ and assume that $n_i \approx n_e \approx n$, then (9) can be rewritten as

$$\mathbf{E} = -\frac{1}{c}\mathbf{v}_i \times \mathbf{B} + \frac{(\mathbf{J} \times \mathbf{B})/c - \nabla \cdot \underline{\mathbf{P}}_e}{en} - \frac{m_e}{e}\frac{d\mathbf{v}_e}{dt}. \tag{10}$$

For the special case of a 2-D system with no y variation, (9) yields

$$E_y = -\frac{1}{c}(v_{ez}B_x - v_{ex}B_z) - \frac{1}{en_e}\left(\frac{\partial P^e_{xy}}{\partial x} + \frac{\partial P^e_{zy}}{\partial z}\right) - \frac{m_e}{e}\left(\frac{\partial v_{ey}}{\partial t} + v_{ex}\frac{\partial v_{ey}}{\partial x} + v_{ez}\frac{\partial v_{ey}}{\partial z}\right). \tag{11}$$

At the X line the magnetic field vanishes, and E_y must be supported by the off-diagonal electron pressure tensor elements or the $-(m_e/e)\partial v_{ey}/\partial t$ inertia term. Figure 5 shows the profile $E_y(x, z = 0)$ (solid line). The term $v_{ex}B_z/c$ is shown by a dashed line (the $-v_{ez}B_x/c$ term vanishes for $z = 0$). This term supports E_y for $|x| \gtrsim 4c/\omega_{pi}$. In the diffusion region, however, $v_{ex}B_z/c$ rises to nearly twice E_y and then drops to zero at the X line. (The ion term $v_{ix}B_z/c$, which is the dominant term in (10) outside of the diffusion region, provides an even poorer representation of E_y in the diffusion region. It increases to a value of about half the maximum of E_y at $|x| \approx 3c/\omega_{pi}$, but it then drops to zero at the X line. Thus it substantially underestimates E_y throughout the diffusion region.) The $(1/en_e)\partial P^e_{zy}/\partial z$ contribution is shown by the dash-dot line, while the $(1/en_e)\partial P^e_{xy}/\partial x$ term is shown by the dotted line. These two terms are generally comparable in size. Near the X line they combine to give the total E_y field (the $(m_e/e)\partial v_{ey}/\partial t$ term is less than 10% of the total E_y), while in the outer diffusion region they, together with the $(m_e/e)v_{ex}\partial v_{ey}/\partial x$ term (shown by a dashed line) reduce the $v_{ex}B_z/c$ contribution down to the net E_y value. Thus the off-diagonal electron pressure terms dominate (by a factor of 2 or greater depending on the value of x) over the electron inertial terms. This is in agreement with results found for a similar reconnection configuration by *Kuznetsova et al.* [1998] in hybrid simulations and by *Hesse and Winske* [1998] in particle simulations. These general results are also in good agreement with the long-standing picture of the nature of the electric field along a neutral line in a collisionless plasma [*Vasyliunas*, 1975].

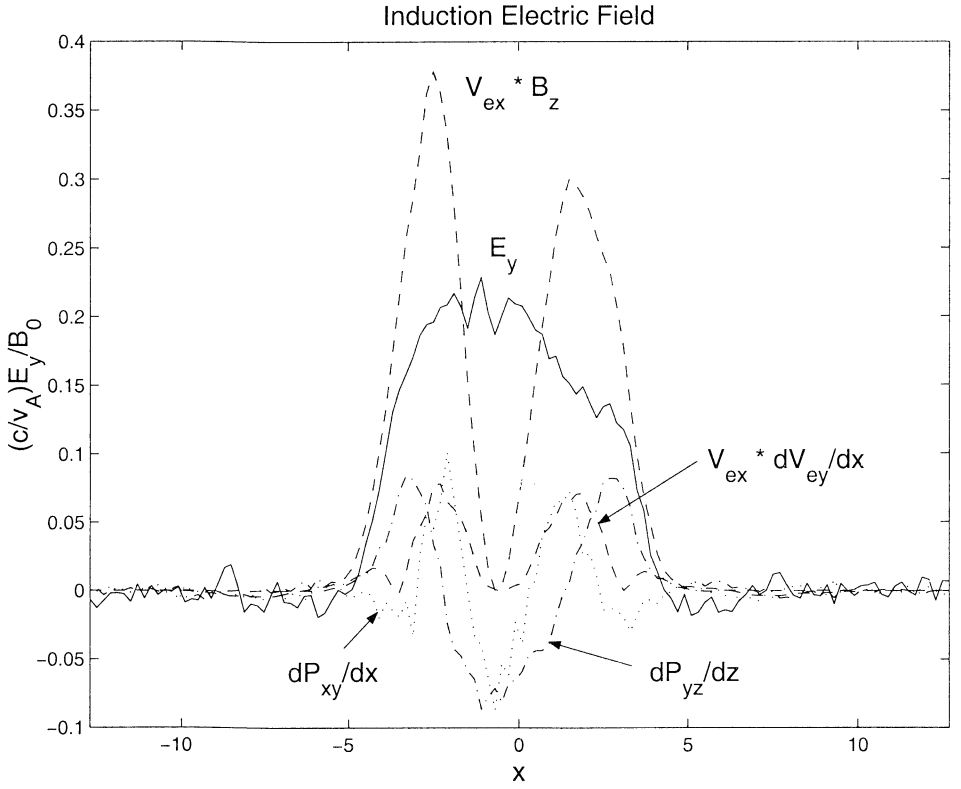

Figure 5. Profile of the inductive electric field E_y averaged over the interval from $\Omega_i t = 15.0$ to 15.6 as a function of x at $z = 0$ (solid line). The additional curves represent the contributions to E_y of individual terms in (11).

The initial flux perturbation (8) has set the scale for the evolution of the current sheet. As the reconnection proceeds, however, the magnetic field perturbation becomes more localized. This is illustrated in Figure 6, which presents a stack plot of $B_z(x, z = 0)$ at equal times over the interval $0 < \Omega_i t \leq 24$. The zero line of the profile is displaced upward by $0.025B_0$ at each successive time. Thus the maximum B_z field is $\approx 0.89B_0$ at $\Omega_i t \approx 21$. As time proceeds, a pulse of B_z propagates away from the X line in each direction; the phase speed of the pulse maximum is $\sim 0.25v_A$. The maximum B_z field continually increases during this interval. At later times the maximum in B_z drops, but here the size of the system and the periodic boundary conditions in x are undoubtedly playing a role.

An additional simulation was run for the same configuration but with a system size only half as large in x ($12.8c/\omega_{pi}$ instead of $25.6c/\omega_{pi}$). Here the inductive E_y reached the same maximum value ≈ 0.25 in a time $\Omega_i t \approx 17$, and the maximum B_z field was about the same as in the larger system. This indicates that the basic reconnection rate is not sensitive to the initial system size. With the smaller initial perturbation length, however, the size in x of the inflow region is cut in half; as a consequence all the outflow speeds are reduced by about a factor of 2. Thus the separation between the maximum and minimum in B_z at a given time is about half as large as in the larger system. The initial system size also affects the final value of $\Delta\psi$. With the smaller system, E_y drops to zero more rapidly after reaching its maximum value; the maximum value of $\Delta\psi$ is then only $1.9B_0c/\omega_{pi}$. Thus a further increase in the system size beyond $L_x = 25.6c/\omega_{pi}$ would allow the reconnection process to continue for a longer time but would probably not lead to stronger fields.

This same half-size configuration was also used to check the sensitivity of the reconnection process to the value of the ion to electron mass ratio. The value was increased to $m_i/m_e = 100$, and the number of grid points in both x and z was doubled so that the grid resolution became $\Delta x = \Delta z = 0.025c/\omega_{pi} = 0.25c/\omega_{pe}$. Figure 7 shows that the time history of the reconnected flux $\Delta\psi$ is almost identical for the two cases of $m_i/m_e = 25$ and 100. The time interval required for $\Delta\psi$ to increase from 0.5 to 1.5 is $\Omega_i t = 5.2$ for $m_i/m_e = 25$ and $\Omega_i t = 4.9$ for $m_i/m_e = 100$. It thus appears that the reconnection rate is essentially independent of m_i/m_e. A similar conclusion was reached by *Hesse et al.* [1999]. With the smaller electron mass, however, the size in z of the region of high-speed electron outflow away from the X line is cut in half, and hence the peak electron speed is essentially doubled, from 1.3 to 2.4 v_A.

The present configuration constitutes an ion-dominated current sheet since the initial y current is carried 5/6

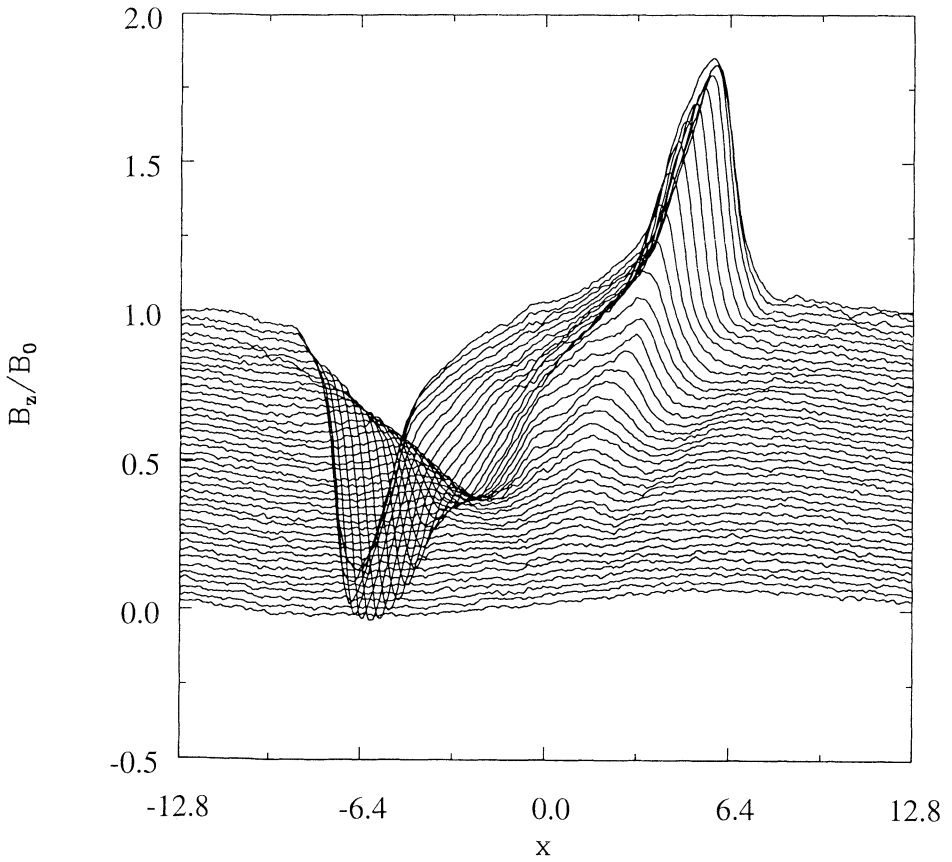

Figure 6. Stack plot of the magnetic field profile $B_z(x, z = 0)$ at equally spaced times during the interval $0 < \Omega_i t \leq 24$. The zero line of the profile is displaced upward by $0.025B_0$ at each successive time.

by the ions and only 1/6 by the electrons. The characteristic reconnection timescales observed in the simulations are quite similar to those obtained by *Kuznetsova et al.* [1998] in simulations of electron-dominated current sheets (which possess an initial E_z electric field to confine the ions) for a system size of $10c/\omega_{pi} \times 5c/\omega_{pi}$ using a hybrid code which incorporated electron quasi-viscous and bulk-flow inertia effects. For the case of an ion-dominated current sheet, however, they found essentially no change in the current sheet configuration over a time period of $\Omega_i t = 24$. This result is strongly at variance with the present results. The previous results for the electron current sheet together with the current results for the GEM ion current sheet suggest that the nature of the current carrier does not have a dramatic effect on the reconnection rate.

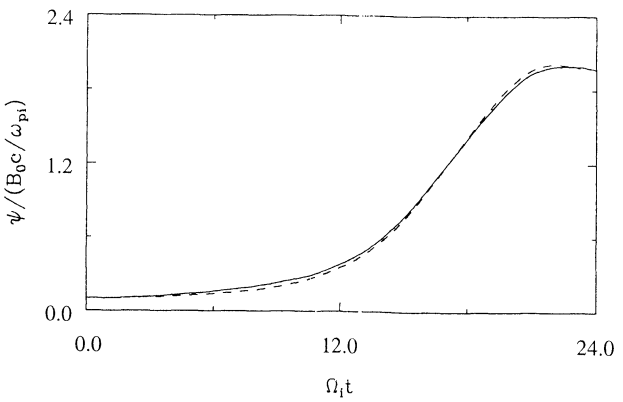

Figure 7. Time history of the reconnected magnetic flux $\Delta\psi$ in a half-size simulation ($L_x \times L_z = 12.8c/\omega_{pi} \times 12.8c/\omega_{pi}$) for values of the ion to electron mass ratio $m_i/m_e = 25$ (solid line) and $m_i/m_e = 100$ (dashed line).

4. Extensions to the GEM Challenge Problem

4.1. Effect of Initial B_{0y} Field

The initial Harris sheet equilibrium is not modified by the addition of a uniform out-of-plane magnetic field component B_{0y}. Such a field is important for reconnection at the magnetopause. Here we examine briefly the effect of such a field on the reconnection process. Again, because of the initial perturbation, the results do not apply to the effects of B_{0y} on the onset of reconnection.

Figure 8 shows the time development of the flux difference $\Delta\psi$ for the case of $B_{0y}/B_0 = 0, 1, 2$. (Note that the choice of $B_{0y} = B_0$ alters the value of the magnetic field rotation across the current sheet from 180°

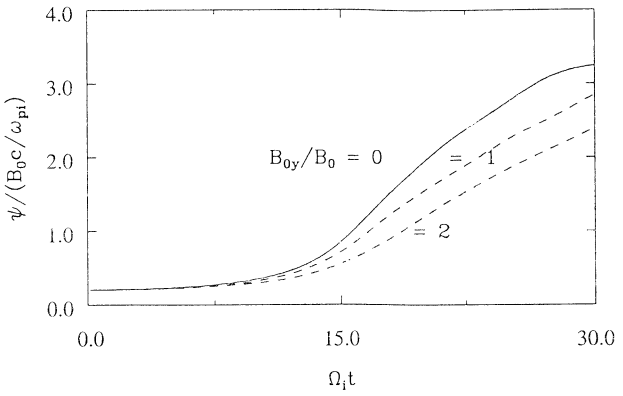

Figure 8. Time history of the reconnected magnetic flux $\Delta\psi$ for three different values of the uniform initial field B_{0y}.

to 90°.) The reconnection rate is evidently reduced by the finite B_{0y}, up to ≈35% for the $B_{0y}/B_0 = 2$ case. A run with $B_{0y}/B_0 = 0.5$ showed essentially no difference in the reconnection rate, so $B_{0y}/B_0 \gtrsim 1$ is necessary to produce an appreciable effect. Since a value of $B_{0y}/B_0 = 0.38$ is sufficient to ensure that $B_{0y} > B_{0x}(z)$ for all $|z| < c/\omega_{pe}$ and thus should significantly alter the electron orbits near the X line, it appears that the overall reconnection rate is not sensitive to the details of the electron physics near the reconnection line.

The presence of the finite B_{0y} destroys the up-down symmetry with respect to $z = 0$. The total B_y field now has a distorted quadrupole pattern (Plate 3a; similar results have been obtained recently by *Karimabadi et al.* [1999]). (Note that the color scale gives the perturbation of B_y relative to the uniform field B_{0y}.) The regions of strongly enhanced B_y are now of larger extent than are those of greatly reduced B_y, and they occupy most of the region inside the magnetic island. They are also connected by a thin strip through the X line. The regions of strongly reduced B_y tend to be concentrated along the separatrix in the second and fourth quadrants; regions of more weakly reduced B_y occupy all of the area exterior to the islands. The peak values of the perturbed B_y ($\lesssim 0.3B_0$) are somewhat stronger

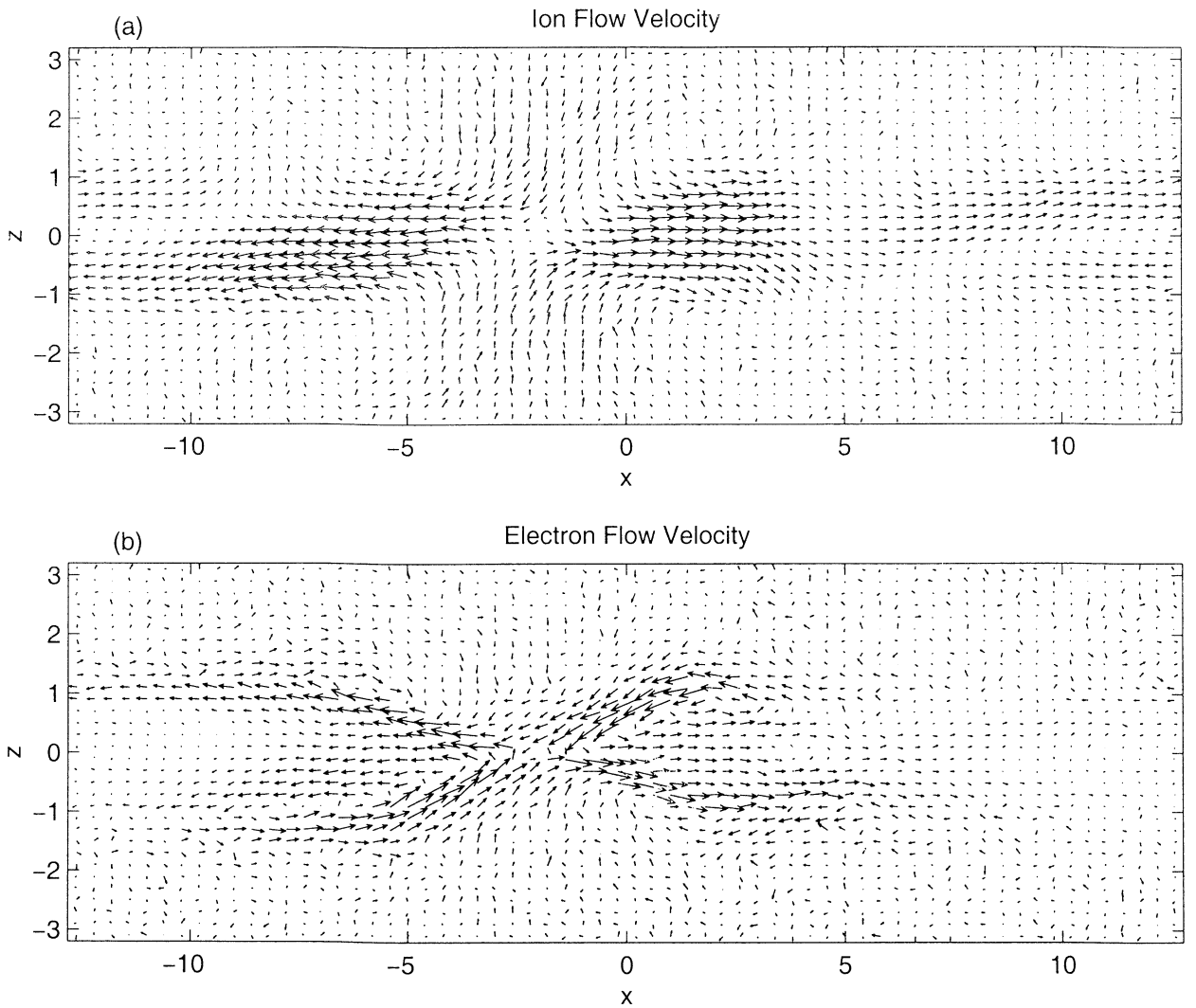

Figure 9. The in-plane (x,z) (a) ion and (b) electron flow velocities at a time when $\Delta\psi = 1.0$ ($\Omega_i t = 16.6$) for the case where $B_{0y}/B_0 = 1.0$.

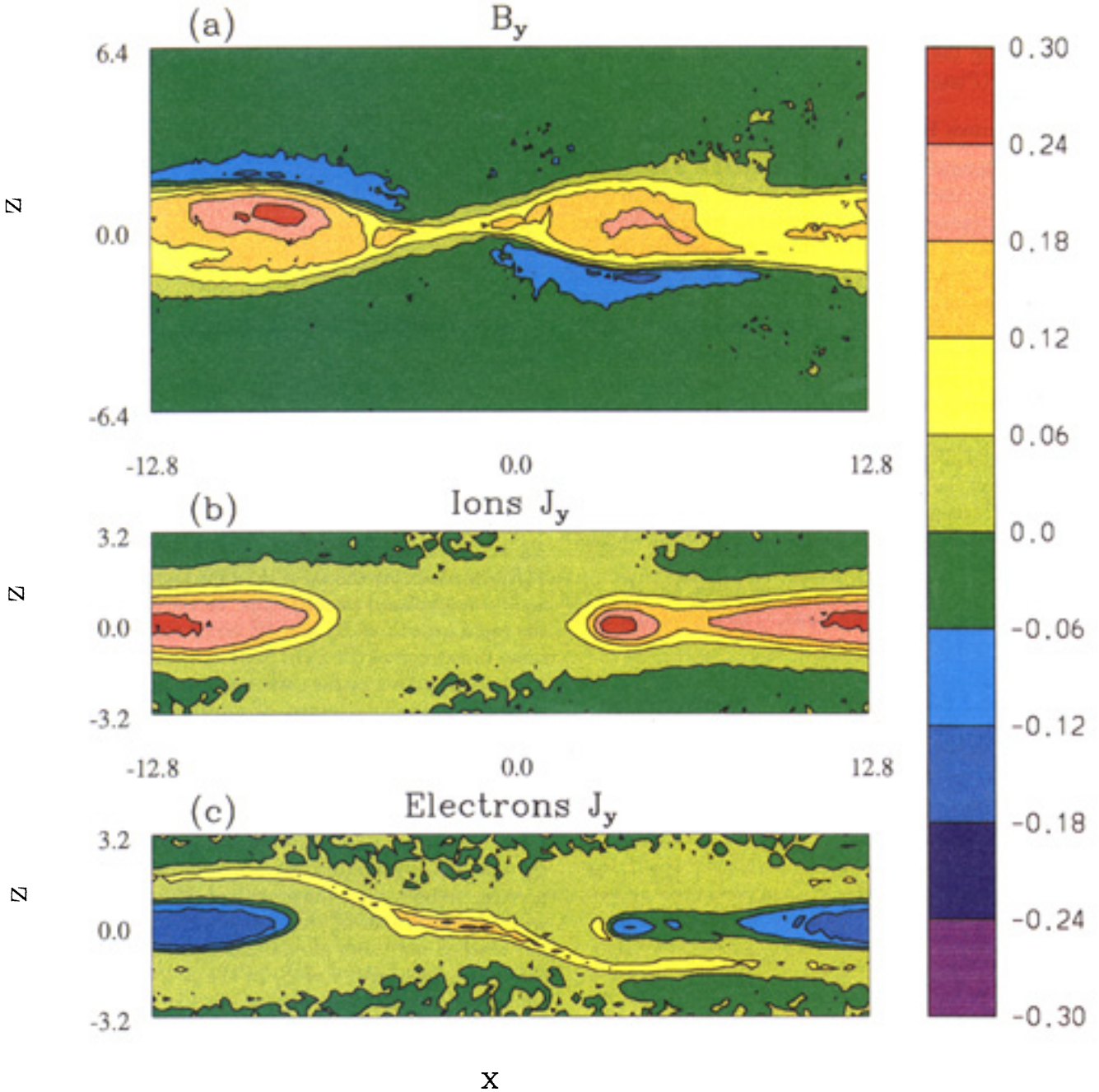

Plate 3. (a) Contours of the perturbed B_y field, and the (b) ion and (c) electron current density J_y at a time when $\Delta\psi = 1.5$ ($\Omega_i t = 19.6$) for the case where $B_{0y}/B_0 = 1.0$.

than in the previous case with $B_{0y} = 0$. While the ion flows remain primarily horizontal out of the diffusion region, the electrons have a strong flow along the separatrix into the diffusion region in the first and third quadrants and a somewhat weaker flow along the separatrix out of the diffusion region in the second and fourth quadrants (Figure 9). The thin region of positive electron J_y current now extends out of the diffusion region along the separatrix in the second and fourth quadrants (Plate 3c).

4.2. Vacuum Reconnection

The configuration considered in section 3 included a background density component n_b (cf. equation (5)). This term represents the asymptotic value of the density away from the neutral sheet such as that in the lobes of the magnetotail, although the value $n_b = 0.2$ is probably too large for this case. In addition, the density floor keeps the Alfvén speed finite everywhere, which is a necessary requirement for the stability of explicit numerical models which neglect the displacement current. The present fully electromagnetic model retains the displacement current, and the Alfvén speed is thus limited by the speed of light. In this section we investigate the effects on the reconnection process of removing the background component ($n_b = 0$). The other parameters are the same as for the simulation described in section 3.

Figure 10 presents time history plots for the total field energies $\int(E_y^2/8\pi)dxdz$, $\int(B_y^2/8\pi)dxdz$, and $\int(B_z^2/8\pi)dxdz$ for the $n_b = 0.2$ (left hand panels) and $n_b = 0$ (right hand panels) runs. In the $n_b = 0.2$ case, the rapid growth of E_y^2 and B_y^2 occur roughly over the same time interval, $12 \lesssim \Omega_i t \lesssim 18$. Thus these two phenomena are driven by the same reconnection process. In contrast, for the $n_b = 0$ case, E_y^2 grows explosively in the short interval of $\Omega_i t \approx 14$–16 and reaches a peak level some 30 times larger than that for $n_b = 0.2$; only subsequently is there any appreciable growth in B_y^2. The peak in B_y^2 occurs only after E_y^2 has collapsed back to zero. Thus the mechanism producing the large B_y^2 in the $n_b = 0$ case is not directly connected with the reconnection. In both cases the growth of B_z^2 begins together with the increase in E_y^2, but the largest B_z^2 energies are not reached until well after the peak in E_y^2. Figure 11 shows the time history of E_y at the X line and the reconnected flux $\Delta\psi$ (cf. Figure 1). The peak value of E_y is ~8 times as large as that for the $n_b = 0.2$ case, while $\Delta\psi$ reaches a value only ~50% larger.

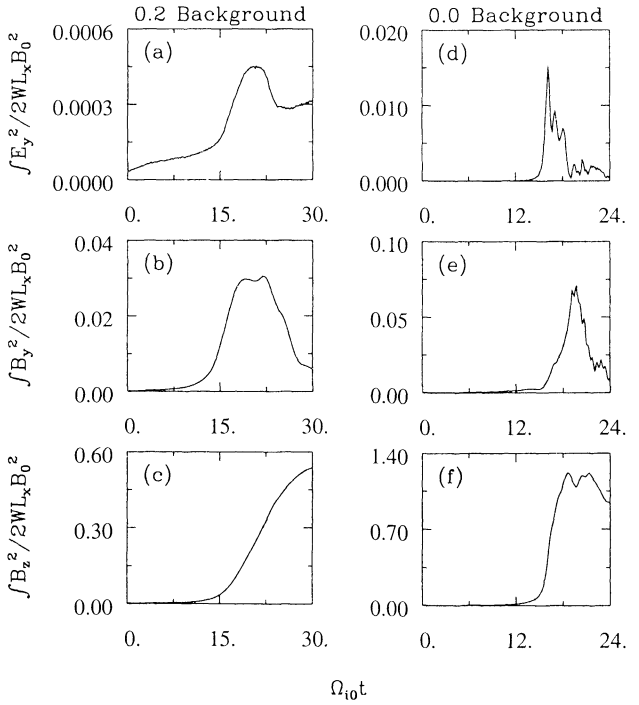

Figure 10. Time history of the total E_y^2, B_y^2, and B_z^2 field energies (left) for the GEM reconnection challenge problem and (right) for the same configuration but with zero background density.

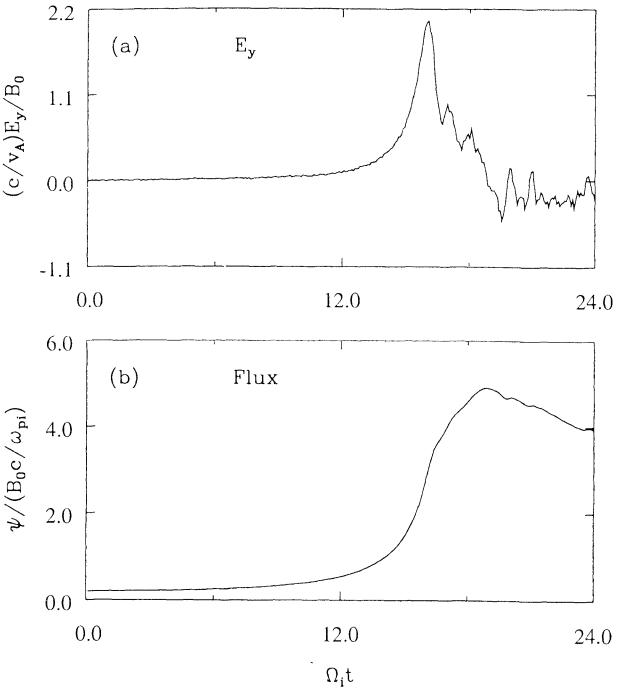

Figure 11. Time history of (a) the inductive electric field E_y at the X line and of (b) the reconnected magnetic flux $\Delta\psi$ in the configuration with zero background density.

The behavior near the X line now contains some significant differences compared with the previous case with $n_b = 0.2$. Figure 12 shows velocity profiles as a function of x for $z = 0$ for a time $\Omega_i t = 15.3$ when $\Delta\psi = 1.8B_0c/\omega_{pi}$. The ion outflow speed is now super-Alfvénic, and the flow profile is similar in shape to that for the electrons with a magnitude roughly two thirds as large. In addition, the density near the X line has dropped to nearly zero. Thus the Hall currents near the X line are greatly reduced, and the resulting B_y field in the diffusion region is much smaller ($< 0.06B_0$) than previously. The stronger B_y fields (up to $0.5B_0$)

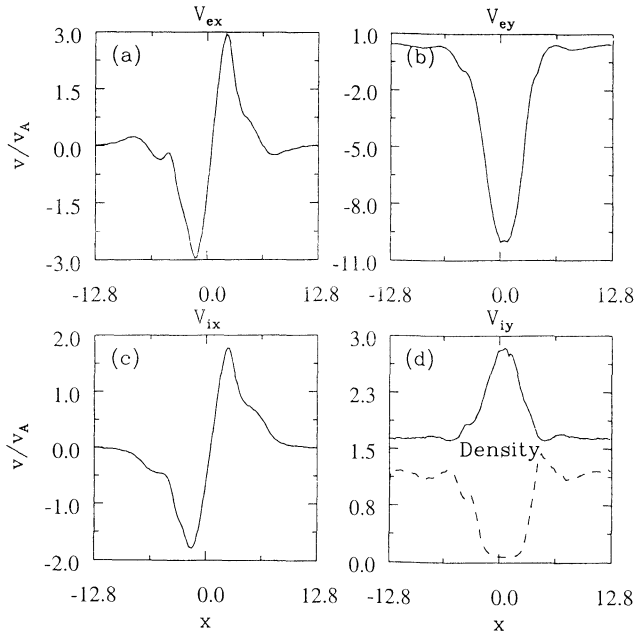

Figure 12. Velocity profiles averaged over the interval from $\Omega_i t = 15.0$ to 15.6 as a function of x at $z = 0$ for (a) electron V_x, (b) electron V_y, (c) ion V_x, and (d) ion V_y in the configuration with zero background density. The dashed line in Figure 12d shows the ion number density as a function of x at the same time.

that develop later are located inside the islands near the edges of the simulation and are probably influenced by the boundary conditions. The stronger E_y field has increased the peak electron drift magnitude in the y direction to $\approx 10 v_A$ and has also resulted in an increase in the ion drift in the diffusion region. The in-plane electron and ion flows at a time $\Omega_i t = 15.8$ when $\Delta\psi = 2.5 B_0 c/\omega_{pi}$ are shown in Figure 13. As the density drops to zero, the plasma is expelled from near the X line, and one approaches the case of vacuum reconnection. The presence of the uniform background density component with $n_b/n_0 \gtrsim 0.1$ thus seems to play a crucial role in determining whether the physics of the diffusion region is dominated by the Hall term and the associated whistler dynamics or approaches the vacuum reconnection case. This explains some previous disparate results [*Mandt et al.*, 1994; *Pritchett*, 1995] that were obtained with and without a background density.

The nature of the inductive electric field is qualitatively similar to the previous case illustrated in Figure 5. Outside of the diffusion region the field is again supported by the $-\mathbf{v}_e \times \mathbf{B}/c$ term. In the outer part of the diffusion region, the $v_{ex} B_z/c$ term exceeds the total E_y field by up to ~30%; near $x = 0$ this term is necessarily small. The $(m_e/e)\partial v_{ey}/\partial t$ and the off-diagonal electron pressure terms are all comparable near $x = 0$ and make positive contributions to E_y. The $(m_e/e) v_{ex} \partial v_{ey}/\partial x$ term again makes a negative contribution to E_y in the outer part of the diffusion region.

5. Summary and Discussion

The GEM magnetic reconnection challenge is designed to determine the physics in the diffusion region around a neutral line that controls the rate of magnetic reconnection in a 2-D configuration. The general results of the various investigations are summarized by *Birn et al.* [this issue]. The results reported in this paper used an electromagnetic particle-in-cell model in which the full particle dynamics were retained for both electrons and ions and Maxwell's equations were solved without approximation. The companion papers report additional studies using a similar particle model [*Hesse et al.*, this issue; *Shay et al.*, this issue], hybrid models in which the electrons are treated as a fluid and the ions as particles [*Kuznetsova et al.*, this issue; *Shay et al.*, this issue], Hall MHD models [*Ma and Bhattacharjee*, this issue; *Birn and Hesse*, this issue; *Otto*, this issue; *Shay et al.*, this issue], and (single-fluid) MHD [*Birn and Hesse*, this issue; *Otto*, this issue]. A number of previous papers have addressed similar issues in 2-D magnetic reconnection. Particle simulations have been performed by *Katanuma and Kamimura* [1980], *Leboeuf et al.* [1982], *Swift* [1986], *Hoshino* [1987], *Hewett et al.* [1988], *Zwingmann et al.* [1990], *Pritchett* [1994], *Horiuchi and Sato* [1994, 1997], *Tanaka* [1995], *Dreher et al.* [1996], *Cai and Lee* [1997], *Shay and Drake* [1998], *Hesse and Winske* [1998], and *Hesse et al.* [1999]. Hybrid simulations addressing the small-scale features of reconnection have been reported by *Hesse et al.* [1995], *Kuznetsova et al.* [1998], *Shay et al.* [1998], and *Karimabadi et al.* [1999], while the consequences of reconnection on a larger scale have been considered by *Krauss-Varban and Omidi* [1995], *Lin and Swift* [1996], *Lin and Xie* [1997], *Lottermoser et al.* [1998], *Nakamura et al.* [1998], and *Krauss-Varban et al.* [1999].

The timescale for reconnection to occur in the GEM problem was observed to be on the order of 10 Ω_i^{-1}, and the corresponding reconnection field is $(c/v_A)(E_y/B_0) \sim 0.24$. In SI units this corresponds to a field $E_y \sim 0.072$ B_0 (nT) (v_A/c). Thus, for a dayside magnetopause configuration with $B_0 \sim 80$ nT and $c/v_A \sim 1000$, $E_y \sim 6$ mV/m; in a magnetotail configuration with $B_0 \sim 20$ nT and $c/v_A \sim 300$, $E_y \sim 5$ mV/m. When these results are combined with previous simulations in which electrons rather than ions were the dominant initial current carrier [*Kuznetsova et al.*, 1998], one concludes that the reconnection rate is at most only weakly dependent on the nature of the current carrier.

The diffusion region was observed to develop a multiscale structure based on electron and ion scale lengths [*Biskamp et al.*, 1997; *Shay et al.*, 1998]. Within a distance of the order of the ion inertial length c/ω_{pi}, the ion motion decouples from that of the electrons, and the ions are accelerated away from the X line. The ion outflow speed remains below the Alfvén velocity. The electrons remain frozen-in to the magnetic field down

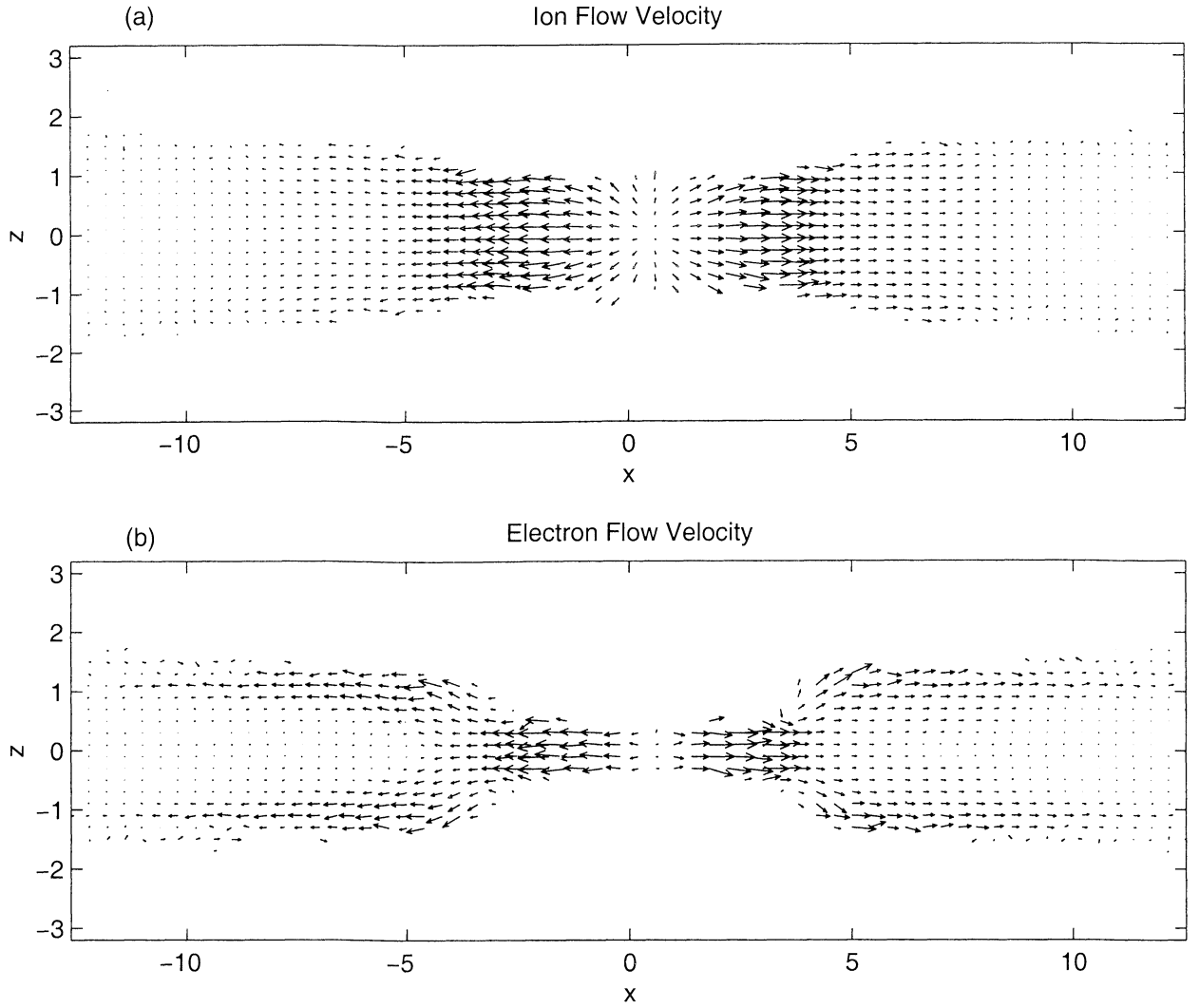

Figure 13. The in-plane (x,z) (a) ion and (b) electron flow velocities at a time when $\Delta\psi = 2.5B_0c/\omega_{pi}$ ($\Omega_i t = 15.8$) for the configuration with zero background density.

to a scale of the order of the electron inertial length c/ω_{pe}. Within this region the electrons are strongly accelerated by the induction electric field E_y, and they are the dominant carrier of the out-of-plane current J_y. The electrons are expelled away from the X line in this region and reach outflow speeds of several times v_A at distances of $\approx 2c/\omega_{pi}$ away from the neutral line.

The difference between the ion and electron dynamics in the diffusion region gives rise to in-plane (Hall) currents which produce an out-of-plane B_y field with a quadrupolar structure [*Sonnerup*, 1979; *Terasawa*, 1983]. The peak B_y field is of the order of 0.2 B_0, and it occurs at $|x| \sim 2.5c/\omega_{pi}$ away from the neutral line. This field pattern is one of the characteristic signatures of the diffusion region when the reconnection physics is dominated by the Hall term and whistler dynamics.

The inductive E_y field, which drives the ion and electron flows into the reconnection region, has a scale in z that is several times larger than c/ω_{pi} and vastly larger than the scale c/ω_{pe} of the thin current region where the frozen-in condition is broken. Thus E_y is relatively slowly varying in the vicinity of the neutral line. In the diffusion region the magnetic field is no longer frozen-in to the electrons, and the simple Ohm's law $\mathbf{E} = -\mathbf{v}_e \times \mathbf{B}/c$ breaks down. It has long been known [*Vasyliunas*, 1975] that the E_y field in a collisionless plasma near the X line must be supported by off-diagonal electron pressure elements and/or electron inertia terms. The present simulations demonstrate explicitly that for spatial scales of the order of c/ω_{pi} the electron pressure terms are the most important. The conclusion that the electron inertia terms are small is further supported by the observation that the nonlinear reconnection rate is only weakly dependent on the electron to ion mass ratio (cf. the companion papers by *Hesse et al.* [this issue] and *Shay et al.* [this issue]. The companion paper by *Shay et al.* [this issue] employs hybrid simulations which include finite electron iner-

tia but assume an isotropic electron pressure. In these simulations the reconnection electric field can only be supported by the electron inertia physics. Nevertheless, the reconnection rate is observed to be almost identical to the present results. This supports the conclusion that the reconnection rate is essentially independent of the specific mechanism which breaks the frozen-in condition [*Shay and Drake*, 1998].

The basic reconnection rate in the nonlinear regime is only weakly dependent on the strength of an initial uniform B_{0y}. A value of $B_{0y}/B_0 \sim 1$ is required before the reconnection rate is reduced appreciably. The presence of a B_{0y} field does alter the symmetry properties of the flows and fields in the diffusion region, but the robustness of the reconnection rate further demonstrates that the reconnection is not sensitive to the details of the microphysics near the reconnection line.

The reconnection rate does change appreciably if the initial background density is low enough (or completely absent) so that the density near the X line drops to a very small value ($\lesssim 0.1 n_0$). In these circumstances, one approaches the case of vacuum reconnection where the underlying physics is no longer controlled by whistler waves. The peak values of E_y and the reconnection rate can then become an order of magnitude larger than in the standard GEM problem.

The GEM reconnection challenge has investigated the physics of magnetic reconnection in a 2-D configuration in a collisionless system using a variety of models: full particle, hybrid, Hall MHD, and single-fluid MHD. In all the models which include the Hall term, the results at length scales much larger than the electron dissipation region are in striking agreement. The reconnection rate is found to be much larger than in the MHD description at large magnetic Reynolds number. Evidently, the underlying whistler and kinetic Alfvén waves facilitate the acceleration of the electrons and ions in the dissipation region much more effectively than the Alfvén waves which dominate the MHD description [*Shay et al.*, 1998; *Shay and Drake*, 1998]. The key remaining task is to extend studies of reconnection to 3-D. Here a much wider variety of kinetic instabilities can develop in the localized current layers in the diffusion region [*Drake et al.*, 1994; *Zhu and Winglee*, 1996; *Pritchett et al.*, 1996; *Drake et al.*, 1997], and these instabilities could significantly alter the magnetic reconnection rate, the structure of the discontinuities which develop outside of the dissipation region, and the distribution of the released magnetic energy.

Acknowledgments. It is a pleasure to thank F. V. Coroniti, J. F. Drake, M. Hesse, M. Kuznetsova, and M. A. Shay for useful and informative discussions regarding the GEM magnetic reconnection challenge. This research was supported by National Science Foundation grant ATM 96-25287 and by NASA grants NAG 5-4339 and NAG 5-3235. The particle simulations were performed at the San Diego Supercomputer Center, which is supported by the National Science Foundation, and at the National Energy Research Scientific Computing Center at the Lawrence Berkeley National Laboratory.

Janet G. Luhmann thanks Dietmar Krauss-Varban and Michael Hesse for their assistance in evaluating this paper.

References

Birn, J., and M. Hesse, GEM magnetic reconnection challenge: Resistive tearing, anisotropic pressure, and Hall effects, *J. Geophys. Res.*, this issue.

Birn, J., et al., Geospace Environment Modeling (GEM) magnetic reconnection challenge, *J. Geophys. Res.*, this issue.

Biskamp, D., E. Schwarz, and J. F. Drake, Two-fluid theory of collisionless magnetic reconnection, *Phys. Plasmas, 4*, 1002, 1997.

Brittnacher, M., K. B. Quest, and H. Karimabadi, On the energy principle and ion tearing in the magnetotail, *Geophys. Res. Lett., 21*, 1591, 1994.

Cai, H. J., and L. C. Lee, The generalized Ohm's law in collisionless magnetic reconnection, *Phys. Plasmas, 4*, 509, 1997.

Drake, J. F., Magnetic reconnection: A kinetic treatment, in *Physics of the Magnetopause, Geophys. Monogr. Ser.*, vol. 90, edited by P. Song, B. U. Ö. Sonnerup, and M. F. Thomsen, p. 155, AGU, Washington, D. C., 1995.

Drake, J. F., R. G. Kleva, and M. E. Mandt, Structure of thin current layers: Implications for magnetic reconnection, *Phys. Rev. Lett., 73*, 1251, 1994.

Drake, J. F., D. Biskamp, and A. Zeiler, Breakup of the electron current layer during 3-D collisionless magnetic reconnection, *Geophys. Res. Lett., 24*, 2921, 1997.

Dreher, J., U. Arendt, and K. Schindler, Particle simulations of collisionless reconnection in magnetotail configuration including electron dynamics, *J. Geophys. Res., 101*, 27,375, 1996.

Furth, H. P., J. Killeen, and M. N. Rosenbluth, Finite-resistivity instabilities of a sheet pinch, *Phys. Fluids, 6*, 459, 1963.

Harris, E. G., On a plasma sheath separating regions of oppositely directed magnetic field, *Nuovo Cimento Soc. Ital. Fis. A-D, 23*, 115, 1962.

Hesse, M., and D. Winske, Electron dissipation in collisionless magnetic reconnection, *J. Geophys. Res., 103*, 26,479, 1998.

Hesse, M., D. Winske, and M. M. Kuznetsova, Hybrid modeling of collisionless reconnection in two-dimensional current sheets: Simulations, *J. Geophys. Res., 100*, 21,815, 1995.

Hesse, M., D. Winske, M. Kuznetsova, J. Birn, and K. Schindler, Hybrid modeling of the formation of thin current sheets in magnetotail configurations, *J. Geomagn. Geoelctr., 48*, 749, 1996.

Hesse, M., K. Schindler, J. Birn, and M. Kuznetsova, The diffusion region in collisionless magnetic reconnection, *Phys. Plasmas, 6*, 1781, 1999.

Hesse, M., J. Birn, and M. Kuznetsova, Collisonless magnetic reconnection: Electron processes and transport modeling, *J. Geophys. Res.*, this issue.

Hewett, D. W., G. E. Frances, and C. E. Max, New regimes of magnetic reconnection in collisionless plasma, *Phys. Rev. Lett., 61*, 893, 1988.

Horiuchi, R., and T. Sato, Particle simulation study of driven magnetic reconnection in a collisionless plasma, *Phys. Plasmas, 1*, 3587, 1994.

Horiuchi, R., and T. Sato, Particle simulation study of collisionless driven reconnection in a sheared magnetic field, *Phys. Plasmas, 4*, 277, 1997.

Hoshino, M., The electrostatic effect for the collisionless tearing mode, *J. Geophys. Res., 92*, 7368, 1987.

Hoshino, M., T. Mukai, T. Yamamoto, and S. Kokubun, Ion dynamics in magnetic reconnection: Comparison between numerical simulation and Geotail observations, *J. Geophys. Res., 103*, 4509, 1998.

Karimabadi, H., D. Krauss-Varban, N. Omidi, and H. X. Vu, Magnetic structure of the reconnection layer and core field generation in plasmoids, *J. Geophys. Res., 104*, 12,313, 1999.

Katanuma, I., and T. Kamimura, Simulation studies of the collisionless tearing instabilities, *Phys. Fluids, 23*, 2500, 1980.

Krauss-Varban, D., and N. Omidi, Large-scale hybrid simulations of the magnetotail during reconnection, *Geophys. Res. Lett., 22*, 3271, 1995.

Krauss-Varban, D., H. Karimabadi, and N. Omidi, Two-dimensional structure of the co-planar and non-coplanar magnetopause during reconnection, *Geophys. Res. Lett., 26*, 1235, 1999.

Kuznetsova, M. M., M. Hesse, and D. Winske, Kinetic quasi-viscous and bulk flow inertia effects in collisionless magnetotail reconnection, *J. Geophys. Res., 103*, 199, 1998.

Kuznetsova, M. M., M. Hesse, and D. Winske, Collisionless reconnection supported by nongyrotropic pressure effects in hybrid and particle simulations, *J. Geophys. Res.*, this issue.

Langdon, A. B., and B. F. Lasinski, Electromagnetic and relativistic simulation models, in *Methods in Computational Physics*, vol. 16, edited by B. Alder et al., p. 327, Academic, San Diego, Calif., 1976.

Laval, G., R. Pellat, and M. Vuillemin, Instabilités electromagnétiques des plasmas sans collisions, in *Plasma Physics and Controlled Fusion Research*, vol. II, p. 259, Int. Atomic Energy Agency, Vienna, 1966.

Leboeuf, J. N., T. Tajima, and J. M. Dawson, Dynamic magnetic x points, *Phys. Fluids, 25*, 784, 1982.

Lembège, B., and R. Pellat, Stability of a thick two-dimensional quasineutral sheet, *Phys. Fluids, 25*, 1995, 1982.

Lin, Y., and D. W. Swift, A two-dimensional hybrid simulation of the magnetotail reconnection layer, *J. Geophys. Res., 101*, 19,859, 1996.

Lin, Y., and H. Xie, Formation of reconnection layer at the dayside magnetopause, *Geophys. Res. Lett., 24*, 3145, 1997.

Lottermoser, R.-F., M. Scholer, and A. P. Matthews, Ion kinetic effects in magnetic reconnection: Hybrid simulations, *J. Geophys. Res., 103*, 4547, 1998.

Ma, Z. W., and A. Bhattacharjee, Hall magnetohydrodynamic reconnection: The GEM challenge, *J. Geophys. Res.*, this issue.

Mandt, M. E., R. E. Denton, and J. F. Drake, Transition to whistler mediated magnetic reconnection, *Geophys. Res. Lett., 21*, 73, 1994.

Nakamura, M. S., M. Fujimoto, and K. Maezawa, Ion dynamics and resultant velocity space distributions in the course of magnetotail reconnection, *J. Geophys. Res., 103*, 4531, 1998.

Otto, A., GEM magnetic reconnection challenge: MHD and Hall MHD—Constant and current dependent resistivity models, *J. Geophys. Res.*, this issue.

Parker, E. N., Sweet's mechanism for merging magnetic fields in conducting fluids, *J. Geophys. Res., 62*, 509, 1957.

Pellat, R., F. V. Coroniti, and P. L. Pritchett, Does ion tearing exist?, *Geophys. Res. Lett., 18*, 143, 1991.

Pritchett, P. L., Effect of electron dynamics on collisionless reconnection in two-dimensional magnetotail equilibria, *J. Geophys. Res., 99*, 5935, 1994.

Pritchett, P. L., The collisionless coalescence instability with two-species and in-plane-current effects, *Phys. Plasmas, 2*, 2664, 1995.

Pritchett, P. L., and F. V. Coroniti, Formation of thin current sheets during plasma sheet convection, *J. Geophys. Res., 100*, 23,551, 1995.

Pritchett, P. L., F. V. Coroniti, and V. K. Decyk, Three-dimensional stability of thin quasi-neutral current sheets, *J. Geophys. Res., 101*, 27,413, 1996.

Quest, K. B., H. Karimabadi, and M. Brittnacher, Consequences of particle conservation along a flux surface for magnetotail tearing, *J. Geophys. Res., 101*, 179, 1996.

Shay, M. A., and J. F. Drake, The role of electron dissipation on the rate of collisionless magnetic reconnection, *Geophys. Res. Lett., 25*, 3759, 1998.

Shay, M. A., J. F. Drake, R. E. Denton, and D. Biskamp, Structure of the dissipation region during collisionless magnetic reconnection, *J. Geophys. Res., 103*, 9165, 1998.

Shay, M. A., J. F. Drake, B. N. Rogers, and R. E. Denton, Alfvénic collisionless magnetic reconnection and the Hall term, *J. Geophys. Res.*, this issue.

Sitnov, M. I., H. V. Malova, and A. S. Sharma, Role of the temperature ratio in the linear stability of the quasi-neutral sheet tearing mode, *Geophys. Res. Lett., 25*, 269, 1998.

Sonnerup, B. U. Ö., Magnetic Field Reconnection, in *Solar System Plasma Physics,* vol. III, edited by L. T. Lanzerotti, C. F. Kennel, and E. N. Parker, p. 45, North-Holland, New York, 1979.

Sweet, P. A., The neutral point theory of solar flares, in *Electromagnetic Phenomena in Cosmical Physics*, edited by B. Lehnert, p. 123, Cambridge Univ. Press, New York, 1958.

Swift, D. W., Numerical simulations of tearing mode instabilities, *J. Geophys. Res., 91*, 219, 1986.

Tanaka, M., Macro-particle simulations of collisionless magnetic reconnection, *Phys. Plasmas, 2*, 2920, 1995.

Terasawa, T., Hall current effect on tearing mode instability, *Geophys. Res. Lett., 10*, 475, 1983.

Vasyliunas, V. M., Theoretical models of magnetic field line merging, 1, *Rev. Geophys. 13*, 303, 1975.

Villasenor, J., and O. Buneman, Rigorous charge conservation for local electromagnetic field solvers, *Comput. Phys. Commun., 69*, 306, 1992.

Wang, J., P. Liewer, and V. Decyk, 3D electromagnetic plasma particle simulations on a MIMD parallel computer, *Comput. Phys. Commun., 87*, 35, 1995.

Yee, K. S., Numerical solution of initial boundary value problems involving Maxwell's equations in isotropic media, *IEEE Trans. Antennas Propag., 14*, 302, 1966.

Zhu, Z., and R. M. Winglee, Tearing instability, flux ropes, and the kinetic current sheet kink instability in the Earth's magnetotail: A three-dimensional perspective from particle simulations, *J. Geophys. Res., 101*, 4885, 1996.

Zwingmann, W., J. Wallace, K. Schindler, and J. Birn, Particle simulation of magnetic reconnection in the magnetotail configuration, *J. Geophys. Res., 95*, 20,877, 1990.

P. L. Pritchett, Department of Physics and Astronomy, University of California, 405 Hilgard Avenue, Los Angeles, CA 90095-1547. (pritchet@physics.ucla.edu)

(Received July 22, 1999; revised September 30, 1999; accepted November 23, 1999.)